Applied Physics Express 15, 061007 (2022)
https://doi.org/10.35848/1882-0786/ac702e

LETTER

AlN quasi-vertical Schottky barrier diode on AlN bulk substrate using $Al_{0.9}Ga_{0.1}N$ current spreading layer

Takuya Maeda[1*], Ryan Page[2], Kazuki Nomoto[3], Masato Toita[4], Huili Grace Xing[1,2,3], and Debdeep Jena[1,2,3]

[1]Kavli Institute at Cornell for Nanoscale Science, Cornell University, Ithaca, NY, 14853, United States of America
[2]Department of Materials Science and Engineering, Cornell University, Ithaca, NY, 14850, United States of America
[3]Department of Electrical and Computer Engineering, Cornell University, Ithaca, NY, 14850, United States of America
[4]Advanced Devices Technology Center, Asahi Kasei Corporation, Hibiya Mitsui Tower, 1-1-2 Yurakucho, Chiyoda-ku, Tokyo 100-8440, Japan

*E-mail: tm654@cornell.edu

Received April 10, 2022; revised April 28, 2022; accepted May 16, 2022; published online May 27, 2022

An aluminum nitride (AlN) quasi-vertical Schottky barrier diode (SBD) was fabricated on an AlN bulk substrate. An undoped AlN layer, a Si-doped $Al_{0.9}Ga_{0.1}N$ current spreading layer and an AlN buffer layer were grown by plasma-enhanced molecular beam epitaxy. The epitaxial AlN layer was etched down to the n-$Al_{0.9}Ga_{0.1}N$ layer to form an Ohmic contact. Ni/Au and V/Al/Ni/Au were deposited on the top AlN layer as Schottky contacts and on the exposed n-$Al_{0.9}Ga_{0.1}N$ layer as Ohmic contacts, respectively. The Ohmic characteristics on the n-$Al_{0.9}Ga_{0.1}N$ layer, capacitance–voltage (C–V) and current–voltage (I–V) characteristics of the AlN SBD were investigated. © 2022 The Japan Society of Applied Physics

Aluminum nitride (AlN) is an ultrawide bandgap semiconductor which has a direct energy bandgap of 6.1 eV, a high piezoelectricity, a high thermal conductivity and a high thermal stability. In addition, AlN can make heterostructures and alloys with GaN and InN. Owing to these attractive properties, AlN-based semiconductors are critical materials for advancing application in deep ultraviolet (DUV) light emitting diodes (LEDs) and laser diodes (LDs).[1–3] AlN is also one of the most promising candidates as a material for high power, high frequency and extremely high-temperature electronic devices, since it is expected to have very high critical electric field (impact ionization and tunneling are well suppressed) and very small intrinsic carrier density owing to its wide bandgap. There are some reports on AlN-based lateral diodes[4–6] and heterojunction field effect transistors.[7–9] Toward the development of AlN electronics, fundamental studies on material science, device process and device physics of AlN are required.

A Schottky barrier diode (SBD) is an essential building block in electronic devices. Irokawa et al. reported Schottky barrier diodes on AlN freestanding substrates.[4] Their device had a lateral structure, and the ideality factor for the forward characteristics was 11.7 at room temperature. Kinoshita et al. reported vertical Schottky barrier diodes on n-type freestanding AlN substrates grown by hydride vapor phase epitaxy (HVPE), with a mobile carrier concentration of 2.4×10^{14} cm^{-3}. A turn on voltage of 2.2 V and the ideality factor of 8 at room temperature were obtained. The breakdown voltages were ranged from 550 to 770 V.[5] Fu et al. demonstrated lateral 2 nm GaN-capped AlN SBDs on sapphire substrates with breakdown voltage over 1 kV.[6] A relatively low ideality factor of 5.5 at room temperature was obtained. In these reports the ideality factors were much far from the unity, indicating that the current transport mechanism departs from ideal thermionic emission and may be dominated by defect-induced components.

Recently, Al-polar AlN bulk single-crystal substrate grown by physical vapor transport (PVT) have become available.[10–13] These substrates exhibit dislocation densities less than 10^4 cm^{-2}, which were used in the demonstration of the first pulsed electrical operation of a UV-C LD.[2] The fabrication of AlN 2 inch wafers has been achieved. Very recently, we developed homoepitaxial growth technology of AlN on an AlN bulk substrate by molecular beam epitaxy (MBE).[14,15] High-quality atomically flat surface can be achieved by homoepitaxy. It is expected that the homoepitaxial high-quality AlN has low density of defects and will allow to access intrinsic material properties and device characteristics in detail. However, currently available AlN substrates are semi-insulating, and it is impossible to fabricate a vertical device using a simple structure with a backside ohmic contact.

In this study, we fabricate an AlN vertical SBD on an AlN bulk substrate using a conductive epitaxial n-type $Al_{0.9}Ga_{0.1}N$ layer. An undoped AlN layer, a Si-doped $Al_{0.9}Ga_{0.1}N$ layer and AlN buffer layer were grown by MBE on an AlN bulk substrate. The top AlN layer was etched down to the $Al_{0.9}Ga_{0.1}N$ layer to form an Ohmic contact on the $Al_{0.9}Ga_{0.1}N$ layer. The device has a quasi-vertical structure:[16] a Schottky electrode on the top AlN layer and a Ohmic electrode on the exposed $Al_{0.9}Ga_{0.1}N$ layer were formed. The Ohmic characteristics on the $Al_{0.9}Ga_{0.1}N$ layer was investigated by transfer length method (TLM). The current–voltage (I–V) and capacitance–voltage (C–V) characteristics of the AlN SBD were measured in the temperature range of 298–573 K using a Signatone probe station coupled with a Keithley 4200 semiconductor parameter analyzer.

Figure 1(a) shows a schematic cross-section of an AlN SBD fabricated in this study. The unintentionally doped 700 nm thick AlN layer, the Si-doped 750 nm thick AlGaN layer with the Al composition of 90%, and the 800 nm thick AlN buffer layer were grown by plasma-assisted MBE on a single-crystal (0001)-oriented AlN bulk substrate provided by Crystal IS. The threading dislocation density of the AlN substrate was 10^3–10^4 cm^{-2}. The AlGaN layer is fully strained and coherently grown on the AlN substrate, confirmed by X-ray diffraction. The band offset between AlN and $Al_{0.9}Ga_{0.1}N$ is very small (~0.2 eV). Figure 1(b) shows the depth profiles of the impurities (Si, O, H and C) in the epitaxial layers measured by secondary ion mass spectrometry (SIMS). The Si concentrations in the top AlN and n-AlGaN layers are under the detection limit ($<5 \times 10^{15}$ cm^{-3}) and 6×10^{19} cm^{-3}, respectively. The O, H and C atoms were unintentionally doped and the concentrations in the AlN and the n-AlGaN layers are almost the same: [O] ~ 7×10^{16} cm^{-3}, [H] < 1×10^{17} cm^{-3}

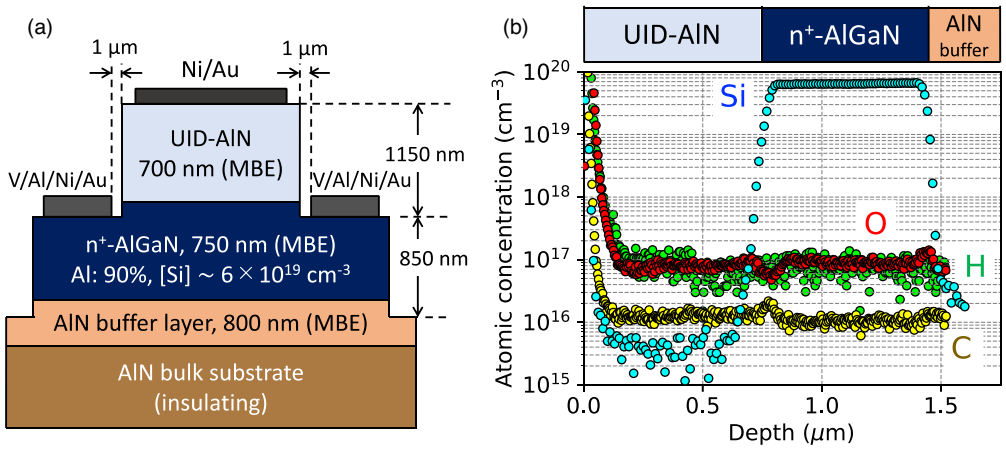

Fig. 1. (Color online) (a) Schematic cross section of an AlN quasi-vertical Schottky barrier diode. A conductive n-AlGaN layer was used as a current spreading layer. (b) The depth profiles of Si, O, H and C atoms in the epitaxial layer obtained by SIMS.

(detection limit) and [C] $\sim 1 \times 10^{16}$ cm^{-3}. The increase near the surface is unreliable due to the surface pollution and the knock-on effect. The top AlN layer was etched down to the AlGaN layer by Cl_2-based inductive coupled plasma-reactive ion etching (ICP-RIE) and mesa isolation structure was formed. The AlGaN layer was also etched down to the AlN buffer layer for device isolation. Before the formation of electrodes, the wafer surface was cleaned by HCl and buffered oxide etch (BOE) for 1 min each. A V/Ni/Al/Au metal stack was deposited on n$^+$-AlGaN for Ohmic electrodes, and rapid thermal annealing (RTA) was performed in 850 °C, N_2 ambient for 5 min. This metal stack and annealing conditions are developed for high Al-composition AlGaN, which was described in the literatures.[17,18] Then Ni/Au stack was deposited as Schottky electrodes.

Figure 2(a) shows the *I*–*V* characteristics of the TLM patterns for the gap lengths from 5 μm to 30 μm. The electrode pads have the 50 μm × 170 μm rectangle shape. Strongly nonlinear behavior is observed at near 0 V. This indicates that the contact is still not good ohmic, since a barrier height at the metal/$Al_{0.9}Ga_{0.1}N$ interface is high and the electron concentration in the $Al_{0.9}Ga_{0.1}N$ layer is low due to the deep donor level (240–290 meV[1,19,20]) and a low activation ratio of Si atoms in Al-rich AlGaN. The resistance was simply extracted as $R = V/I$ at the current level of 10 mA. Figure 2(b) shows the resistance at 10 mA as a function of a gap length at room temperature. From the slope and intercept, the sheet resistance (R_{sh}) and the contact resistance (R_c) were extracted as 32 kΩ/square and 1.7 kΩ, respectively. It should be noted that the *I*–*V* characteristics are nonlinear, and these values are very rough estimations. The specific length (L_t) and specific contact resistivity (ρ_c) at 0.01 A are 9.0 μm and 0.026 Ω cm^2, respectively. Figure 2(c) shows the *I*–*V* characteristics of the TLM patterns for the gap length of 5 μm from 298 K to 573 K. The current increased with elevating temperature. However, the Schottky-like nonlinearity remains at high temperature. Figure 2(d) shows the temperature dependence of the R_{sh} and R_c extracted at the current level of 10 mA. Both R_{sh} and R_c rapidly decreased with elevating temperature. The reduction of R_{sh} indicates that enhanced ionization of donors in the AlGaN layer at higher temperature (the donor level for Si atoms in $Al_{0.9}Ga_{0.1}N$ is deep and not fully ionized at room temperature). The reduction of R_c may originate from enhanced thermionic emissions via the metal/$Al_{0.9}Ga_{0.1}N$ interface. The improvement of Ohmic characteristics for Al-rich AlGaN is a critical issue in AlN-based electronics in the future.

Figure 3(a) shows the *C*–*V* characteristics of the AlN SBD in the $1/C^2$–*V* plot. The relatively low frequency of 50–100 kHz was used in the measurements due to large series resistance. In the measured voltage range, the loss tangent was sufficiently low (<0.05), and no frequency dependence was observed in these frequency range. Near the built-in potential of about 3 V, the plots have steep slope and rapidly increased with decreasing applied voltage. From +1 V to −10 V, the capacitance is almost constant but with a very small slope. These indicate that the top AlN layer was fully depleted owing to low net donor density and the voltage dependence of the capacitance under reverse bias detected the depletion in the n-AlGaN layer. The net donor concentration ($N_d - N_a$) can be obtained using the following equation,

$$N_d - N_a = -\frac{2}{e\varepsilon_s\left(\frac{dC^{-2}}{dV}\right)A^2}. \quad (1)$$

Here, N_d and N_a are the donor and acceptor concentrations, e is elementary electron charge. A is the device area, and ε_s is the dielectric constant along the c-axis in AlN. In this study, the value of 9 ε_0 [21,22] was used. Figure 3(b) shows the depth profile of the net donor concentration in the epitaxial layer. The measured region is limited to near the top AlN/n-AlGaN heterostructure interface owing to the very low donor concentration in the top AlN layer (<3×10^{15} cm^{-3}). The top AlN thickness of 670–700 nm and the average net donor concentration in the n-AlGaN layer of 4.2×10^{17} cm^{-3} were obtained. The top AlN thickness obtained by the *C*–*V* measurement is consistent with that obtained by SIMS. However, the net donor (mobile carrier) concentration in the n-AlGaN layer is two orders of magnitude lower than the Si concentration. This result indicates that (1) not all Si atoms act as donors in Al-rich AlGaN layer and/or (2) there are deep level defects that act as compensation acceptors.

Figure 4(a) shows the *I*–*V* characteristics of the AlN SBD at room temperature in a linear plot. A clear rectifying characteristic with a turn-on voltage of approximately 3 V is observed. This turn-on voltage is consistent with the built-in potential obtained by the *C*–*V* measurement. These values are reasonable,

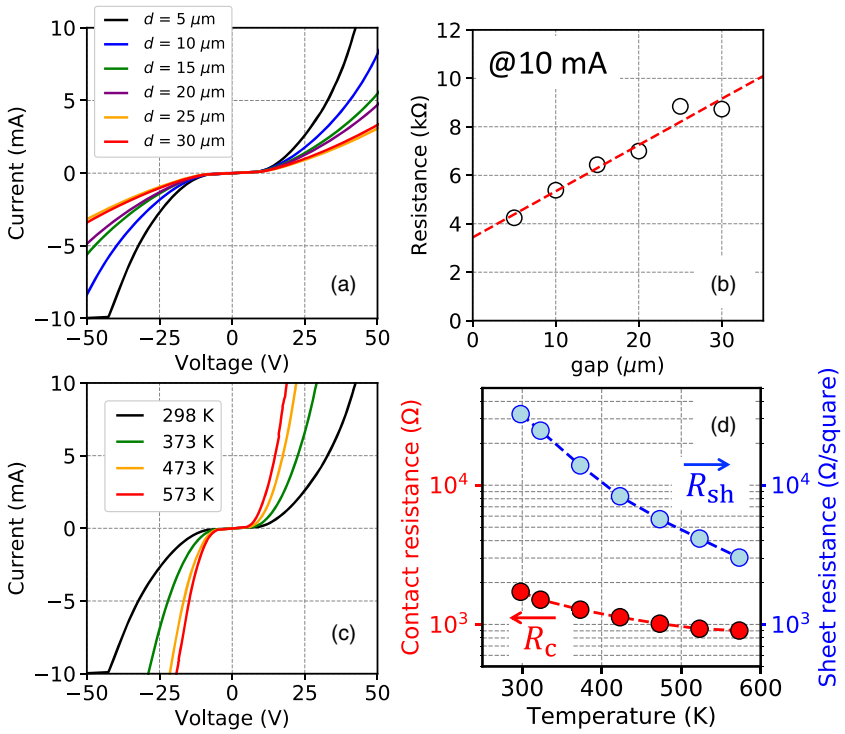

Fig. 2. (Color online) (a) The *I*–*V* characteristics for 170 μm × 50 μm TLM patterns with the gap lengths from 5 μm to 30 μm. (b) The resistance versus the gap at 10 mA. (c) The *I*–*V* characteristics of the TLM patterns with the gap length of 5 μm from 298 K to 573 K. (d) The temperature dependence of the contact resistance and the sheet resistance extracted at 10 mA.

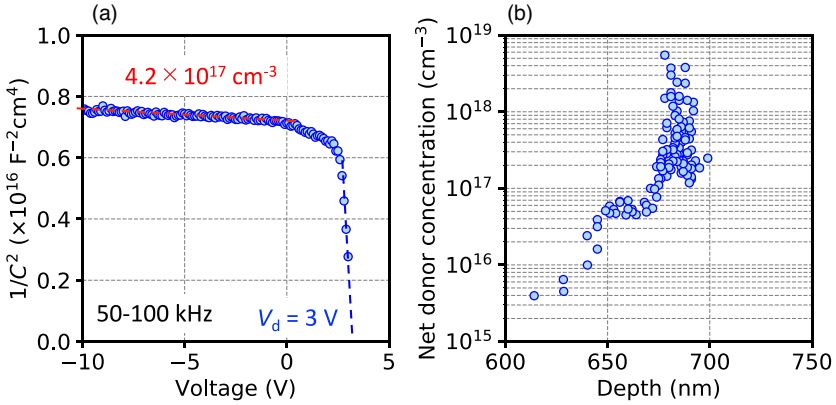

Fig. 3. (Color online) (a) The *C*–*V* characteristics of the AlN SBD in the $1/C^2$–*V* plot. (b) The depth profile of the net donor concentration in the epitaxial layer extracted from the *C*–*V* characteristics.

considering the barrier height of Ni/n-AlN of 3.1–3.5 eV reported recently.[23,24] Figure 4(b) shows the forward *I*–*V* characteristics of the AlN SBD at 298–573 K. The temperature-independent subthreshold slope (300 mV dec^{-1}) is observed in the measured temperature range. The on-resistance was very high (e.g. 1.8 Ω cm^2 at 298 K) and decreased with elevating temperature (e.g. 0.1 Ω cm^2 at 573 K). This large on-resistance is mostly dominated by the contact resistance at the metal/n-AlGaN interface. The forward *I*–*V* characteristics were analyzed based on the thermionic emission model. The current density based on the thermionic emission is expressed as

$$J = J_0\left[\exp\left(\frac{eV}{nkT}\right) - 1\right], J_0 = A^*T^2\exp\left(-\frac{e\phi_b}{kT}\right), \quad (2)$$

where J_0 and n are the saturation current density and the ideality factor, respectively. A^* is the effective Richardson constant. In this study, electron effective mass of 0.32 m_0 ($A^* = 38.4$ A K^{-2} cm^{-2})[25] was used. From the analysis of J_0 using $e\phi_b = kT \cdot \ln(A^*T^2/J_0)$, the barrier height ($e\phi_b$) can be obtained. If the additional current components such as tunneling current or defect-induced current are not negligible, the ideality factor comes to deviate from unity and it cause the underestimation of the barrier height. Figure 4(c) shows the temperature dependence of the ideality factor and the *apparent* barrier height extracted from the forward *I*–*V* characteristics. The ideality factor was much larger than unity and decreased with elevating temperature (e.g. 5.0 at 298 K and 2.5 at 573 K). This large ideality factor originates from an additional current component which is larger than the thermionic emission dominates the transport and a large series resistance. The origin of the forward current may be a defect-induced transport and should be investigated in the future. The apparent barrier height increased with elevating temperature, since the effect of the overestimation of J_0

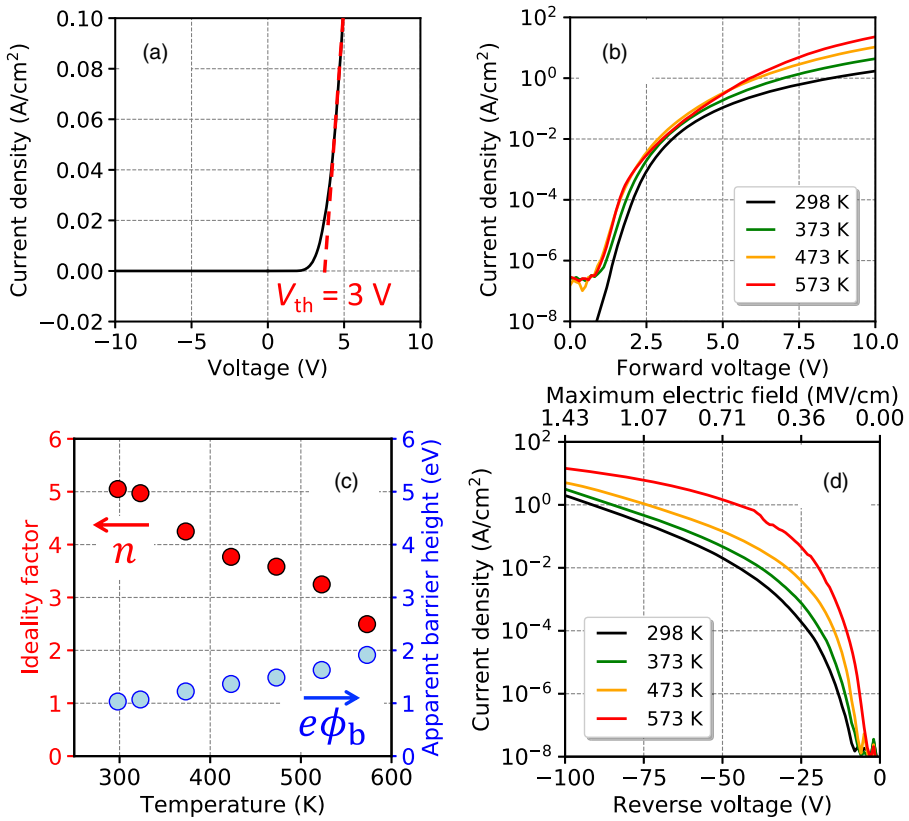

Fig. 4. (Color online) (a) The *I–V* characteristics of the AlN SBD at 298 K in a linear plot. (b) The forward *I–V* characteristics of the AlN SBD from 298 K to 573 K. (c) The temperature dependence of the ideality factor and the *apparent* barrier height extracted from the forward *I–V* characteristics. (d) The reverse *I–V* characteristics of the AlN SBD from 298 K to 573 K.

becomes smaller at higher temperature. These tendencies were also observed in heteroepitaxial GaN SBDs with a large ideality factor.[26,27] To investigate the temperature dependence of Schottky barrier height accurately, a nearly ideal SBD which shows a temperature-independent ideality factor close to unity is needed.[28] Figure 4(d) shows the reverse *I–V* characteristics of the AlN SBD at 298–573 K. The device showed breakdown voltage higher than at least 100 V, although the device has no edge termination structure. The reverse leakage current increased with reverse voltage, and the leakage current was higher at high temperature. In other wide-bandgap semiconductors such as 4H-SiC, GaN and Ga_2O_3, it is well known that the mechanism of reverse leakage current is thermionic field emission: tunneling of thermal electrons via a Schottky interface under high electric field.[29–34] However, the value calculated based on the thermionic field emission using the analytical model in the literature[30] and the parameters (maximum electric field of 1.43 MV cm^{-1}, barrier height of 3 eV[23,24] and electron effective mass of 0.32 m_0[25]) was very low (2×10^{-38} A cm^{-2}). Therefore, the reverse leakage current in the AlN SBD cannot be explained by the thermionic field emission. The origin of the leakage current may be defect-induced component and should be investigate in the future.

In conclusion, we demonstrated the AlN quasi-vertical SBD on a bulk AlN substrate using the buried conductive n-AlGaN layer, and the ohmic characteristics on the n-AlGaN layer, *I–V* and *C–V* characteristics of the AlN SBD were investigated at 298–573 K. The device showed clear rectification with turn-on voltage of about 3 V. The series resistance of the device was high (1.8 Ω cm^2), which was mostly dominated by the large contact resistance at the metal/n-AlGaN interface. The ideality factor was 5 at room temperature. The reverse leakage current was much higher than the expected thermionic field emission current. These results indicate that the both forward and reverse current transports are still non-ideal and may be dominated by a defect-induced transport. The development of good ohmic contact for n-type AlGaN with a high Al composition as well as the further improvement of crystal quality of an epitaxial AlN layer on an AlN bulk substrate are essential toward the future AlN electronics.

Acknowledgments This work is partially supported by ULTRA, an Energy Frontier Research Center funded by the U.S. Department of Energy (DOE), Office of Science, Basic Energy Sciences (BES), under Award No. DE-SC0021230. The authors also acknowledge the Cornell Nanoscale Facility (CNF) for device fabrication, supported by the National Science Foundation with grant No. NNCI-1542081. The author also thanks to Kavli Institute at Cornell (KIC) for nanoscale science and Japan Society for the Promotion of the Science (JSPS).

ORCID iDs Takuya Maeda https://orcid.org/0000-0002-2736-5611

1) Y. Taniyasu, M. Kasu, and T. Makimoto, Nature **441**, 325 (2006).
2) Z. Zhang, M. Kushimoto, T. Sakai, N. Sugiya, A, L. Schowalter, C. Sasaoka, and H. Amano, Appl. Phys. Express **12**, 124003 (2019).
3) S. Tanaka et al., Appl. Phys. Express **14**, 055505 (2021).
4) Y. Irokawa, E. A. Villora, and K. Shimamura, Jpn. J. Appl. Phys. **51**, 040206 (2012).
5) T. Kinoshita et al., Appl. Phys. Express **8**, 061003 (2015).
6) H. Fu, I. Baranowski, X. Huang, H. Chen, Z. Lu, J. Montes, X. Zhang, and Y. Zhao, IEEE Electron Device Lett. **38**, 1286 (2017).
7) H. Okumura, S. Suihkonen, J. Lemettinen, A. Uedono, Y. Zhang, D. Piedra, and T. Palacios, Jpn. J. Appl. Phys. **57**, 04FR11 (2018).
8) A. Hickman, R. Chaudhuri, S. J. Bader, K. Nomoto, K. Lee, H. G. Xing, and D. Jena, IEEE Electron Device Lett. **40**, 1293 (2019).

9) K. Nomoto et al., IEDM Tech. Digest, 2020, p. 8.3.1, 10.1109/IEDM13553.2020.9371994.
10) P. Lu, R. Collazo, R. F. Dalmau, G. Durkaya, N. Dietz, B. Raghothamachar, M. Dudley, and Z. Sitar, J. Cryst. Growth **312**, 58 (2009).
11) M. Bickermann, B. M. Epelbaum, O. Filip, P. Heimann, S. Nagata, and A. Winnacker, Phys. Status Solidi C **7**, 21 (2010).
12) Y. Kumagai et al., Appl. Phys. Express **5**, 055504 (2012).
13) R. T. Bondokov, S. G. Mueller, K. E. Morgan, G. A. Slack, S. Schujman, M. C. Wood, J. A. Smart, and L. J. Schowalter, J. Cryst. Growth **310**, 4020 (2008).
14) Y. J. Cho, C. S. Chang, K. Lee, M. Gong, K. Nomoto, M. Toita, L. J. Schwalter, D. A. Muller, D. Jena, and H. G. Xing, Appl. Phys. Lett. **116**, 172106 (2020).
15) K. Lee, Y. J. Cho, L. J. Schowalter, M. Toita, H. G. Xing, and D. Jena, Appl. Phys. Lett. **116**, 262102 (2020).
16) Y. Zhang, M. Sun, D. Piedra, M. Azize, X. Zhang, T. Fujishima, and T. Palacios, IEEE Electron Device Lett. **35**, 618 (2014).
17) K. Mori, K. Takeda, T. Kusafuka, M. Iwaya, T. Takeuchi, S. Kamiyama, I. Akasaki, and H. Amano, Jpn. J. Appl. Phys. **55**, 05FL03 (2016).
18) B. B. Haidet, B. Sarkar, P. Reddy, I. Bryan, Z. Bryam, R. Kirste, R. Collazo, and Z. Sitar, Jpn. J. Appl. Phys. **56**, 100302 (2017).
19) Y. Taniyasu, M. Kasu, and T. Makimoto, Appl. Phys. Lett. **85**, 4672 (2004).
20) M. Kanechika and T. Kachi, Appl. Phys. Lett. **88**, 202106 (2006).
21) S. Strite and H. Morkoc, J. Vac. Sci. Technol. B **10**, 1237 (1992).
22) M. Kazan, S. Pereira, M. R. Correia, and P. Masri, J. Appl. Phys. **106**, 023523 (2009).
23) Y. Kurosaki and H. Okumura, Presented at the 67th Japan Society of Applied Physics Spring Meeting, 13a-B401-6.
24) M. Hiroki, Y. Taniyasu, and K. Kumakura, Presented at the 68th Japan Society of Applied Physics Spring Meeting, 16a-Z16-3.
25) I. Vurgaftman, J. R. Meyer, and L. R. Ram-Mohan, J. Appl. Phys. **89**, 5815 (2001).
26) N. Yıldırım, K. Ejderha, and A. Turut, J. Appl. Phys. **108**, 114506 (2010).
27) Y. Zhou, D. Wang, C. Ahyi, C.-C. Tin, J. Williams, M. Park, N. M. Williams, A. Hanser, and E. A. Preble, J. Appl. Phys. **101**, 024506 (2007).
28) T. Maeda, M. Okada, M. Ueno, Y. Tamamoto, T. Kimoto, M. Horita, and J. Suda, Appl. Phys. Express **10**, 051002 (2017).
29) F. A. Padovani and R. Stratton, Solid-State Electron. **9**, 695 (1996).
30) T. Hatakeyama and T. Shinohe, Mater. Sci. Forum **389–393**, 1169 (2002).
31) M. Hara, S. Asada, T. Maeda, and T. Kimoto, Appl. Phys. Express **13**, 041001 (2020).
32) J. Suda, K. Yamaji, Y. Hayashi, T. Kimoto, K. Shimoyama, H. Namota, and S. Nagao, Appl. Phys. Express **3**, 101003 (2010).
33) W. Li, D. Saraswat, Y. Long., K. Nomoto, D. Jena, and H. G. Xing, Appl. Phys. Lett. **116**, 192101 (2020).
34) T. Maeda, M. Okigawa, Y. Kato, I. Takahashi, and T. Shinohe, AIP Adv. **10**, 125119 (2020).